# Strain-Optic Law for Orthotropic Model Materials

R. PRABHAKARAN*
*Indian Institute of Technology, Kanpur, India*

**A strain-optic law for orthotropic birefringent model materials, based on the concept of Mohr circle of birefringence, is developed. The strain-fringe value, like the stress-fringe value, is influenced by the fiber orientation angle and the ratio of the principal strains. The strain-optic law is experimentally verified by testing a unidirectionally glass fiber reinforced circular disk under diametral compression. It is shown that an average strain-fringe value can be used in strain analysis of orthotropic models and the resultant error is less than 20% in most cases. A similar attempt to use an average stress-fringe value leads to much larger errors. The measured isoclinic parameters are found to give the principal strain directions to a very good approximation. It is proposed that orthotropic photoelastic models can be treated as isotropic models to obtain an approximate strain analysis by employing the strain-optic law and an average strain-fringe value.**

## Nomenclature

| | |
|---|---|
| $E$ | = Young's modulus |
| $f_\sigma$ | = stress-fringe value |
| $f_\varepsilon$ | = strain-fringe value |
| $G$ | = shear modulus |
| $L$ | = direction of major amount of reinforcement in the composite |
| $N$ | = fringe order per unit thickness of model |
| $N_L, N_T, N_{LT}$ | = stress-birefringence components |
| $N'_L, N'_T, N'_{LT}$ | = strain-birefringence components |
| $T$ | = direction transverse to the $L$-direction in the plane of the composite |
| $\alpha$ | = angle between major principal stress and $L$-direction |
| $\beta$ | = angle between major principal strain and $L$-direction |
| $\gamma$ | = shear strain |
| $\varepsilon$ | = normal strain |
| $\nu$ | = Poisson's ratio |
| $\sigma$ | = normal stress |
| $\tau$ | = shear stress |
| $\theta'$ | = optical isoclinic parameter from the stress-optic law |
| $\theta''$ | = optical isoclinic parameter from the strain-optic law |
| $\phi$ | = angle between direction of diametral compressive load on disk and $L$-axis |

*Subscripts*

| | |
|---|---|
| 1 | = major principal stress- or strain-direction |
| 2 | = minor principal stress- or strain-direction |

## Introduction

THE extension of transmission photoelastic techniques to glass fiber reinforced plastics has received increasing attention in recent years. Pih and Knight[1] attempted to interpret the isochromatic and isoclinic fringes by simple stress-strain models. Sampson[2] postulated a Mohr circle of birefringence and developed a stress-optic law. This stress-optic law was found to agree with the isochromatic results of Ref. 1 quite well, but the agreement with the isoclinic results of Ref. 1 was poor. Dally and Prabhakaran[3] developed a simple method of fabricating orthotropic model materials and developed a uniaxial stress-optic law based on simple stress-strain models. They also showed that Sampson's result could be derived from this stress-optic law and solved[4] simple problems in orthotropic elasticity involving uniaxial stress-fields. Bert[5] applied the well-established Bhagavantam theory of photoelasticity for the orthorhombic crystalline system to two-dimensional analysis of filamentary composites and derived expressions which were similar in form to those obtained by Sampson earlier. The author[6] later fabricated a much improved model material and solved another example involving uniaxial stress-fields.

The author[7] verified the general stress-optic law developed by Sampson for special cases of biaxial stress-fields and presented[8] new experimental results which verified the Mohr circle of birefringence concept in the case of isoclinics also. Pipes and Rose[9] attempted to develop a strain-optic law for orthotropic model materials. They started with the assumption that a single strain-optic coefficient was sufficient to characterize an orthotropic model material and concluded that the assumption was valid for the model material fabricated by them, which contained 3% reinforcement by volume.

In this paper, a general strain-optic law is developed for orthotropic model materials. The development is very similar to that adapted by Sampson for the stress-optic law and is based on the concept of a Mohr circle of birefringence. The strain-optic law is verified for the case of a circular disk fabricated from unidirectionally reinforced composite subjected to diametral compression. From an examination of the general strain-optic law, it is proposed that orthotropic models can be analyzed in the same manner as isotropic models by utilizing an average strain-fringe value; the errors resulting from the approximation are less than 20% in most cases.

## Strain-Optic Law

For isotropic model materials the isochromatic fringe order can be interpreted in terms of either the difference in principal stresses, $(\sigma_1 - \sigma_2)$, or the difference in principal strains, $(\varepsilon_1 - \varepsilon_2)$. The relationship between the stress-fringe value, $f_\sigma$ (psi-in./fringe), and the strain-fringe value, $f_\varepsilon$ (in./fringe), is given by

$$f_\varepsilon = \frac{1+\nu}{E} f_\sigma \tag{1}$$

where $\nu$ is the Poisson's ratio and $E$ is Young's modulus. The stress-optic law for orthotropic model materials is now fully developed but the isochromatic fringe order does not give the principal stress difference directly; therefore it is necessary to separate the principal stresses by the shear difference method based on Mohr circle of birefringence. This is quite tedious and besides results in considerable error due to the numerical integration procedure.

The dependence of the stress-fringe value (for uniaxial stress-fields) and the Young's modulus on the fiber orientation angle is shown in Fig. 1. Because of the similarity in the shape of the two curves and in view of Eq. (1), it may be expected that the

Received March 15, 1974; revision received October 29, 1974.
Index categories: Structural Composite Materials (Including Coatings); Structural Static Analysis.

* Assistant Professor, Department of Mechanical Engineering.

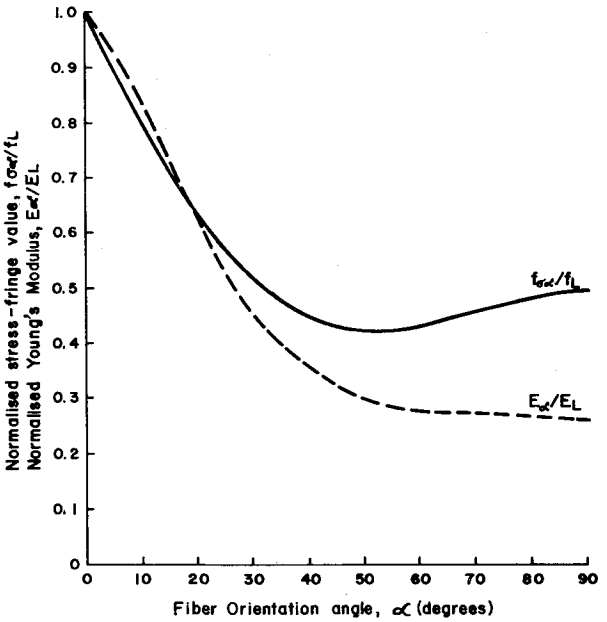


**Fig. 1 Dependence of uniaxial stress-fringe value and Young's modulus on the fiber orientation angle.**

dependence of the strain-fringe value on the fiber orientation angle will be less than that of the stress-fringe value. The stress-strain relations for an orthotropic material, referred to its material symmetry axes, can be written as

$$\varepsilon_L = \frac{\sigma_L}{E_L} - \frac{\nu_{TL}}{E_T}\sigma_T \tag{2}$$

$$\varepsilon_T = \frac{\sigma_T}{E_T} - \frac{\nu_{LT}}{E_L}\sigma_L \tag{3}$$

$$\gamma_{LT} = \frac{\tau_{LT}}{G_{LT}} \tag{4}$$

where $L$ refers to the major reinforcement direction and $T$ is the direction perpendicular to $L$. The Mohr circle of stress-birefringence is represented by

$$N^2 = (N_L - N_T)^2 + (N_{LT})^2 \tag{5}$$

where the birefringence components are given[2] in terms of the stresses by

$$N_L = \sigma_L/f_L, \quad N_T = \sigma_T/f_T, \quad N_{LT} = 2\tau_{LT}/f_{LT} \tag{6}$$

and $f_L$, $f_T$, $f_{LT}$ are the principal stress-fringe values.

Solving for the stresses from the Eqs. (2–4) and substituting in Eq. (6), it is possible to write the birefringence components in terms of the strains as

$$\begin{aligned} N_L &= \frac{E_L}{1-\nu_{LT}\nu_{TL}}\frac{\varepsilon_L + \nu_{TL}\varepsilon_T}{f_L} \\ N_T &= \frac{E_T}{1-\nu_{LT}\nu_{TL}}\frac{\nu_{LT}\varepsilon_L + \varepsilon_T}{f_T} \\ N_{LT} &= 2(G_{LT}/f_{LT})\gamma_{LT} \end{aligned} \tag{7}$$

Substituting Eqs. (7) into Eq. (5), and defining strain-birefringence components

$$N'_L = \varepsilon_L/f_{\varepsilon L}, \quad N'_T = \varepsilon_T/f_{\varepsilon T}, \quad N'_{LT} = \gamma_{LT}/f_{\gamma LT} \tag{8}$$

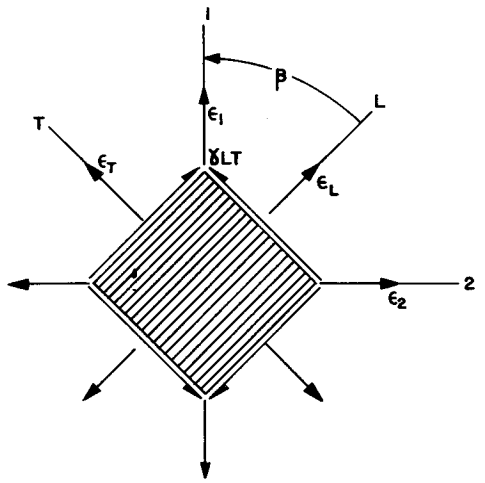


**Fig. 2 Coordinate axes and strain notation.**

the Mohr circle of strain-birefringence can be represented by

$$N^2 = (N'_L - N'_T)^2 + (N'_{LT})^2 \tag{9}$$

The strain-fringe values, $f_{\varepsilon L}$, $f_{\varepsilon T}$, and $f_{\gamma LT}$ are given in terms of the stress-fringe values and the elastic constants by

$$\begin{aligned} f_{\varepsilon L} &= \frac{1-\nu_{LT}\nu_{TL}}{E_L/f_L - E_T\nu_{LT}/f_T} \\ f_{\varepsilon T} &= \frac{1-\nu_{LT}\nu_{TL}}{E_T/f_T - E_L\nu_{TL}/f_L} \\ f_{\gamma LT} &= f_{LT}/2G_{LT} \end{aligned} \tag{10}$$

For the unidirectionally reinforced E-glass polyester model material used in this investigation and described fully elsewhere,[6] the elastic and photoelastic properties are given in Table 1. For isotropic model materials the Mohr circles of stress-birefringence and strain-birefringence become equivalent and Eqs. (10) simplify to Eq. (1).

Considering an element of the model material, shown in Fig. 2, the principal strains $\varepsilon_1$ and $\varepsilon_2$ can be transformed onto the material symmetry axes $L$ and $T$ to give components

$$\begin{aligned} \varepsilon_L &= \varepsilon_1 \cos^2\beta + \varepsilon_2 \sin^2\beta \\ \varepsilon_T &= \varepsilon_1 \sin^2\beta + \varepsilon_2 \cos^2\beta \\ \gamma_{LT} &= (\varepsilon_1 - \varepsilon_2)\sin 2\beta \end{aligned} \tag{11}$$

Combining Eqs. (8), (9) and (11), it is possible to write

$$N = \frac{\varepsilon_1}{f_{\varepsilon L}}\left\{\left[\left(\cos^2\beta + \frac{\varepsilon_2}{\varepsilon_1}\sin^2\beta\right) - \left(\sin^2\beta + \frac{\varepsilon_2}{\varepsilon_1}\cos^2\beta\right)\frac{f_{\varepsilon L}}{f_{\varepsilon T}}\right]^2 + \left[\left(1 - \frac{\varepsilon_2}{\varepsilon_1}\right)\frac{f_{\varepsilon L}}{f_{\gamma LT}}\sin 2\beta\right]^2\right\}^{1/2} \tag{12}$$

The relationship between the isochromatic response and the state of strain, Eq. (12), is very similar to that between $N$ and the state of stress developed by Sampson.

When $\varepsilon_2 = 0$, Eq. (12) simplifies to

$$f_{\varepsilon\beta} = f_{\varepsilon L}\left\{\left(\cos^2\beta - \frac{f_{\varepsilon L}}{f_{\varepsilon T}}\sin^2\beta\right)^2 + \frac{f_{\varepsilon L}^2}{f_{\gamma LT}^2}\sin^2 2\beta\right\}^{-1/2} \tag{13}$$

where the notation $f_{\varepsilon\beta} = \varepsilon_1/N$ is adopted. The variation of $f_{\varepsilon\beta}$ with $\beta$ is shown in Fig. 3. Although Eq. (13) is similar to the corresponding uniaxial form of the stress-optic law

**Table 1 Comparison of properties of two different orthotropic model materials**

| Material | $E_L$ | $E_T$ ($\times 10^6$ psi) | $G_{LT}$ | $\nu_{LT}$ | $f_L$ | $f_T$ (psi-in./fr) | $f_{LT}$ | $f_{\varepsilon L}$ | $f_{\varepsilon T}$ ($\times 10^{-3}$ in./fringe) | $f_{\gamma LT}$ | $(f_\varepsilon)_{av}$ |
|---|---|---|---|---|---|---|---|---|---|---|---|
| *E*-glass polyester | 4.15 | 1.30 | 0.50 | 0.29 | 890 | 445 | 395 | 0.255 | 0.390 | 0.395 | 0.345 |
| *S*-glass epoxy | 0.380 | 0.195 | 0.058 | 0.33 | 100 | 60 | 40 | 0.347 | 0.359 | 0.345 | 0.351 |

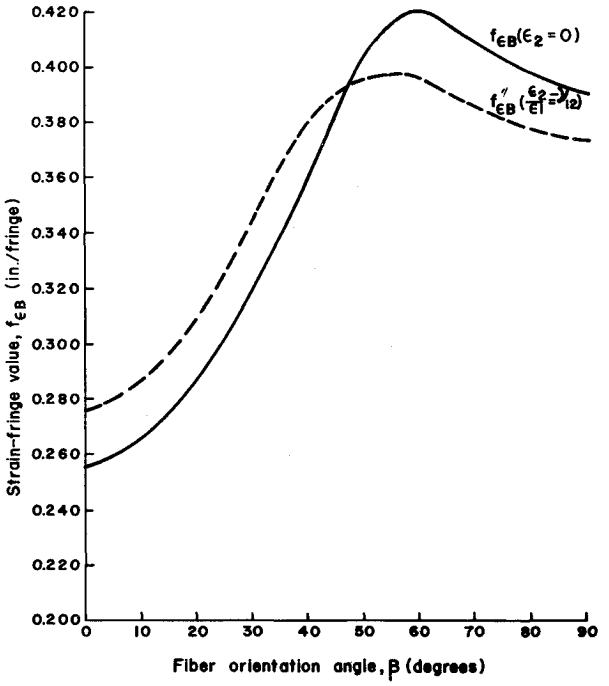


Fig. 3 Dependence of uniaxial and biaxial strain-fringe value on the fiber orientation angle.

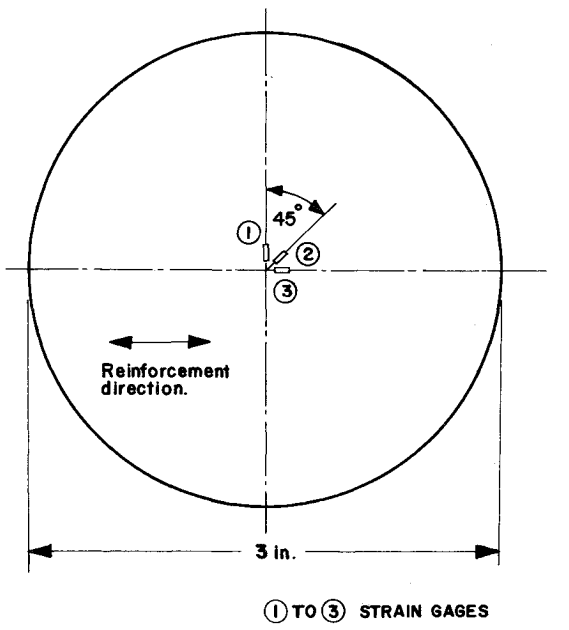


Fig. 4 Schematic diagram of the orthotropic disk model with strain gages.

developed by Sampson there is an important difference in using it. Whereas $f_{\sigma x}$ can be measured by applying a uniaxial stress to the calibration specimen, the direct measurement of $f_{\varepsilon\beta}$ requires the application of stresses in two mutually perpendicular directions; these stresses should be of the same sign and properly adjusted so that the Poisson effect is counteracted. Also, the stresses should be applied in the proper directions with respect to the fiber direction because the principal stress and strain directions, in general, are different for anisotropic materials.

The calibration procedure is simplified by considering the application of a single stress and allowing for the Poisson effect. In this case $\varepsilon_2/\varepsilon_1 = -\nu_{12}$ and

$$f'_{\varepsilon\beta} = (1+\nu_{12})f_{\varepsilon L}\left\{\left[(\cos^2\beta - \nu_{12}\sin^2\beta) - (\sin^2\beta - \nu_{12}\cos^2\beta)\frac{f_{\varepsilon L}}{f_{\varepsilon T}}\right]^2 + \left[(1+\nu_{12})\frac{f_{\varepsilon L}}{f_{\gamma LT}}\sin 2\beta\right]^2\right\}^{-1/2} \tag{14}$$

where the notation

$$f'_{\varepsilon\beta} = \frac{\varepsilon_1 - \varepsilon_2}{N} = \frac{\varepsilon_1(1+\nu_{12})}{N}$$

is adopted. The nonprincipal elastic constant $\nu_{12}$ is given by

$$\nu_{12} = \frac{E_1}{E_L}\left[\nu_{LT} - \tfrac{1}{4}\left(1 + 2\nu_{LT} + \frac{E_L}{E_T} - \frac{E_L}{G_{LT}}\right)\sin^2 2\beta\right] \tag{15}$$

where

$$\frac{E_L}{E_1} = \cos^4\beta + \frac{E_L}{E_T}\sin^4\beta + \frac{1}{4}\left(\frac{E_L}{G_{LT}} - 2\nu_{LT}\right)\sin^2 2\beta \tag{16}$$

The variation of $f'_{\varepsilon\beta}$ with $\beta$ is shown in Fig. 3. The maximum difference between $f_{\varepsilon\beta}$ and $f'_{\varepsilon\beta}$ is less than about 6%. In this case also, the angle between the major principal strain (and not the applied major principal stress) and the fiber direction should be used in Eq. (14).

## Experimental Verification

To verify the general strain-optic law, represented by Eq. (12), a series of tests were conducted. A circular disk, 3 in. in diameter, was machined from a unidirectionally reinforced *E*-glass polyester plate of 0.2-in. thickness. The disk was annealed at about 100°C for two hours after machining, to remove the birefringence due to the machining stresses. A rectangular strain gage rosette was mounted at the center of the disk, as shown in Fig. 4. The disk was loaded in diametral compression and the angle between the direction of the load and the fiber direction, $\phi$, was varied from 0° to 90° in steps of 15°. At each value of $\phi$, the load was increased in steps and the corresponding values of strain and fringe order at the center of the disk were noted. Values of strain and fringe order were averaged at each value of $\phi$ by plotting them against the load and the values corresponding to a load of 1000 lb. were used in the analysis. The residual birefringence due to the fabrication procedure was accounted for in interpreting the observed isochromatic fringe order as described in another paper.[6]

The principal strains and their directions were computed from the strain gage readings. The principal strain difference and

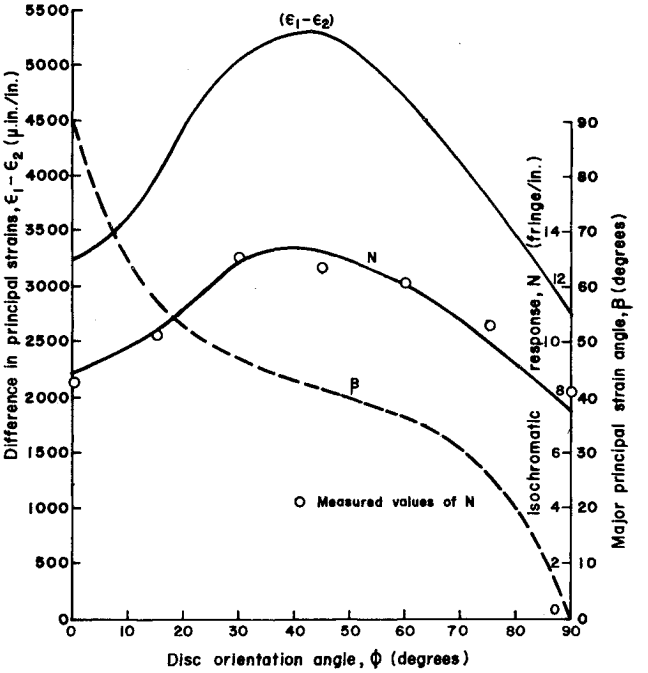


Fig. 5 Variation of $(\varepsilon_1 - \varepsilon_2)$, $N$, and $\beta$ with the disk orientation angle.

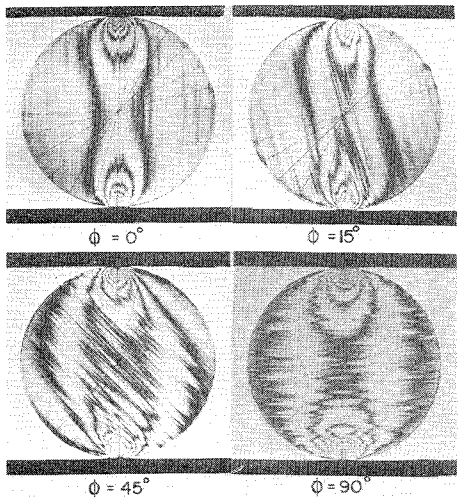


**Fig. 6 Selected light-field isochromatic fringe patterns of the circular disk model under diametral compression.**

the major principal strain direction are shown in Fig. 5 as a function of $\phi$. These values were substituted in Eq. (12) and the fringe order per unit thickness of the model, $N$, was computed. The computed values of $N$ are also shown in Fig. 5. The measured values of $N$ are in good agreement with the values obtained from the strain-optic law, thus verifying Eq. (12).

The isochromatic fringe patterns exhibited a general similarity to the corresponding patterns for isotropic models but for values of $\phi$ other than 0° and 90°, an asymmetry was noticeable. Selected light-field isochromatic fringes shown in Fig. 6, illustrate this point.

## Simplified Strain-Optic Law

Pipes and Rose[9] attempted to develop a strain-optic law for orthotropic model materials but they assumed from the very beginning that a single strain-fringe value was sufficient to characterize the material. The material fabricated by them was far from homogenous (macroscopically) in that it consisted of a few central layers of fibers sandwiched between thick resin layers and besides, the volume fraction of the fibers was as low as 3%. An average strain-fringe value of $0.351 \times 10^{-3}$ in./fringe was given for the material. As shown in the previous section of this paper, the three principal strain-fringe values can be different for a realistic model material containing as much as 35% by volume of fibers.

As already indicated in this paper, the uniaxial stress-fringe value and the Young's modulus exhibit a very similar variation with the fiber orientation angle and this fact may be expected to result in a smaller variation of the strain-fringe value with $\beta$. The general expression for the strain-fringe value is obtained from Eq. (12) and the isotropic form of the strain-optic law

$$\varepsilon_1 - \varepsilon_2 = N f_\varepsilon \tag{17}$$

as

$$f_\varepsilon = \left\{\left[\left(\cos^2\beta + \frac{\varepsilon_2}{\varepsilon_1}\sin^2\beta\right) - \left(\sin^2\beta + \frac{\varepsilon_2}{\varepsilon_1}\cos^2\beta\right)\frac{f_{\varepsilon L}}{f_{\varepsilon T}}\right]^2 + \left[\left(1 - \frac{\varepsilon_2}{\varepsilon_1}\right)\frac{f_{\varepsilon L}}{f_{\gamma LT}}\sin 2\beta\right]^2\right\}^{1/2} \tag{18}$$

The strain-fringe value, $f_\varepsilon$, is shown as a function of $\beta$ for different values of $\varepsilon_2/\varepsilon_1$ in Fig. 7. By convention $\varepsilon_1 \geqq \varepsilon_2$ and so only the range $-\infty \leqq (\varepsilon_2/\varepsilon_1) \leqq 1$ is considered. The average strain-fringe value, $(f_\varepsilon)_{av}$, for normalizing $f_\varepsilon$ is obtained from the average of the three principal strain-fringe values $f_{\varepsilon L}$, $f_{\varepsilon T}$ and $f_{\gamma LT}$. For the material under investigation, $(f_\varepsilon)_{av}$ is $0.345 \times 10^{-3}$ in./fringe.

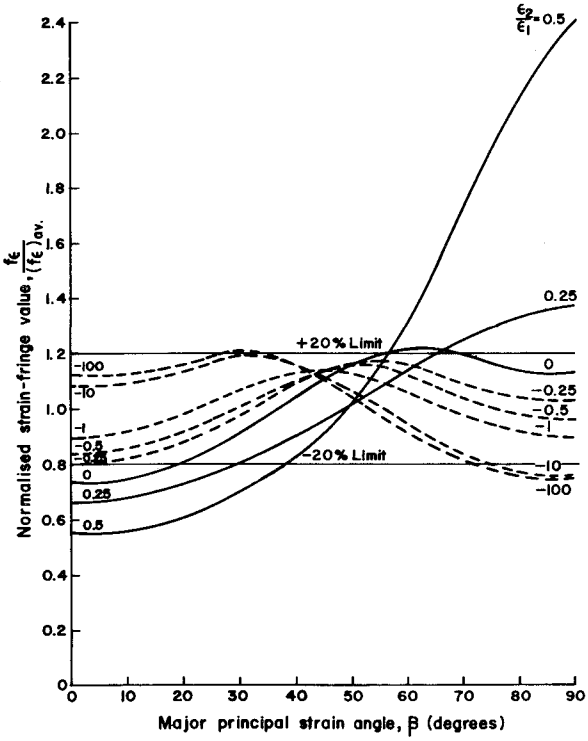


**Fig. 7 Dependence of biaxial strain-fringe value on the fiber orientation angle and the principal strain ratio.**

In Fig. 7, the limits for $\pm 20\%$ deviations from unity are also drawn. From this figure it is clear that $f_\varepsilon = 0$ for all $\beta$ when $\varepsilon_1/\varepsilon_2 = 1$. This is because, unlike in isotropic models, in orthotropic models $N$ is not equal to 0 when $\varepsilon_2/\varepsilon_1 = 1$ as $f_{\varepsilon L}$ and $f_{\varepsilon T}$ are not equal generally. However, the curves for most of the other values of $\varepsilon_2/\varepsilon_1$ and $\beta$ lie within the band for $f_\varepsilon/(f_\varepsilon)_{av} = 0.8$ and $f_\varepsilon/(f_\varepsilon)_{av} = 1.2$. It is interesting to note that the curves for $\varepsilon_2/\varepsilon_1 \leqq 0$ conform to this pattern very well and in

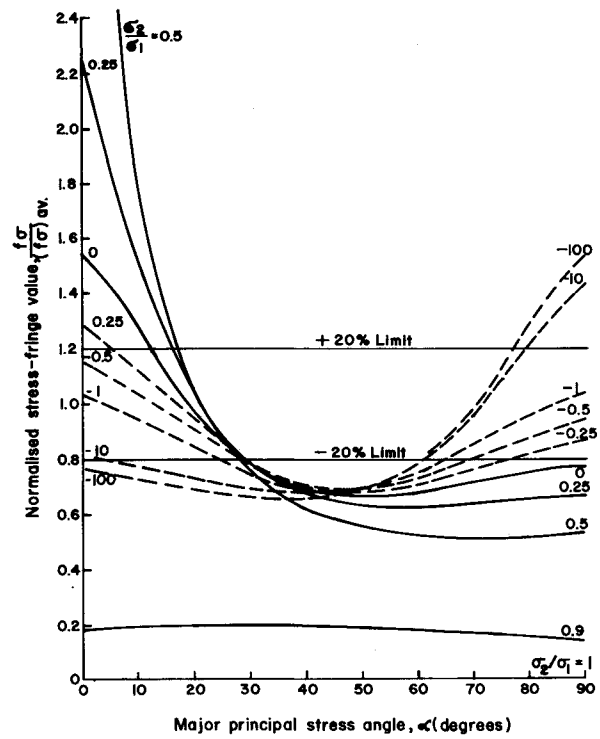


**Fig. 8 Dependence of biaxial stress-fringe value on the fiber orientation angle and the principal stress ratio.**

particular, the curves for $\varepsilon_2/\varepsilon_1 = -10$ and $\varepsilon_2/\varepsilon_1 = -100$ are very close to each other.

The expectation, on the basis of Fig. 1, that the strain-fringe value would be more or less constant may not be fulfilled completely, as seen in Fig. 7. However, the variation of the stress-fringe value, $f_\sigma$, as a function of $\alpha$ for various values of $\sigma_2/\sigma_1$ (between $-\infty$ and 1) is shown in Fig. 8. The average stress-fringe value, $(f\sigma)_{av}$, for normalizing $f_\sigma$ is obtained from the average of the three principal stress-fringe values $f_L$, $f_T$ and $f_{LT}$; this value is 575 psi-in./fringe for the material under investigation. The general features of Fig. 8 are similar to those of Fig. 7 (for instance, $f_\sigma = 0$ for all $\beta$ when $\sigma_2/\sigma_1 = 1$) but the $\pm 20\%$ limits do not contain a major portion of the curves. Therefore, comparing Figs. 7 and 8, the expectation of a constant $f_\varepsilon$ can be said to be partially fulfilled.

The variations of the principal strain-difference and the fringe order per unit thickness with the disk orientation angle, $\phi$, in Fig. 5 are seen to be quite similar. The principal strain-differences for different disk orientations (all corresponding to a diametral compressive load of 1000 lb) are shown against computed values of $N$ in Fig. 9. It is seen that the points lie quite close to a straight line through the origin whose slope gives a strain-fringe value of $0.375 \times 10^{-3}$ in./fringe. This value is quite close to the $(f_\varepsilon)_{av}$ value of $0.345 \times 10^{-3}$ in./fringe. It may be noted that the ratio of principal strains ranged from $-0.91$ -- $-6.20$ and from Fig. 7 the concept of an average strain-fringe value is found to hold good for this range of $\varepsilon_2/\varepsilon_1$.

For the sake of comparison, the difference in principal stresses for the different disk orientations (corresponding to a diametral compressive load of 1000 lb) are also shown against computed values of $N$ in Fig. 9. The principal stresses and their orientations were calculated from the strain gage readings, and the biaxial form of the stress-optic law similar to Eq. (12), was used to calculate $N$. The values of $N$ computed from the strain-optic law and the stress-optic law agreed very well. From Fig. 9 it is observed that there is a considerable scatter in the values of $(\sigma_1 - \sigma_2)$ about an average straight line through the origin. The slope of this straight line gives a stress-fringe value of 445 psi-in./fringe which is much different from the $(f_\sigma)_{av}$ value of 575 psi-in./fringe. The ratio of principal stresses ranged from $-0.7$ -- $-17.0$. As mentioned in connection with Fig. 8, there appears to be no basis for visualizing an average stress-fringe value.

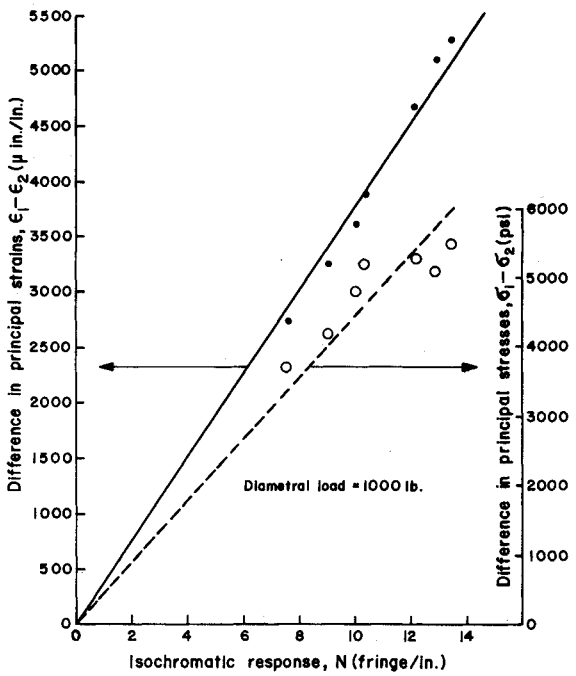


Fig. 9 Variation of $(\varepsilon_1 - \varepsilon_2)$ and $(\sigma_1 - \sigma_2)$ with $N$ for different disk orientations.

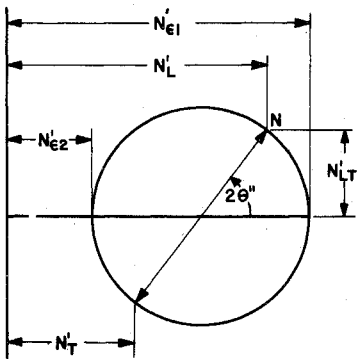


Fig. 10 Mohr circle of strain-birefringence.

From the Mohr circle of strain-birefringence it is also possible to derive an expression for the optical isoclinic parameter. From Fig. 10, it is possible to write

$$\tan 2\theta'' = N'_{LT}/N'_L - N'_T = \frac{\gamma_{LT}/f_{\gamma LT}}{\varepsilon_L/f_L - \varepsilon_T/f_T} \tag{19}$$

where $\theta''$ is the optical isoclinic parameter from the Mohr circle of strain-birefringence. Substituting the transformation equations, Eqs. (11), into Eq. (19),

$$\tan 2\theta'' = \frac{f_{\varepsilon L}\left(1 - \dfrac{\varepsilon_2}{\varepsilon_1}\right)\sin 2\beta}{f_{\gamma LT}\left[\left(\cos^2\beta + \dfrac{\varepsilon_2}{\varepsilon_1}\sin^2\beta\right) - \dfrac{f_{\varepsilon L}}{f_{\varepsilon T}}\left(\sin^2\beta + \dfrac{\varepsilon_2}{\varepsilon_1}\cos^2\beta\right)\right]} \tag{20}$$

When a uniaxial stress is applied to calibration specimens of different fiber orientations, $\varepsilon_2/\varepsilon_1 = -\nu_{12}$ and Eq. (20) becomes

$$\tan 2\theta'' = \frac{f_{\varepsilon L}(1+\nu_{12})\sin 2\beta}{f_{\gamma LT}\left[(\cos^2\beta - \nu_{12}\sin^2\beta) - \dfrac{f_{\varepsilon L}}{f_{\varepsilon T}}(\sin^2\beta - \nu_{12}\cos^2\beta)\right]} \tag{21}$$

where $\nu_{12}$ is given by Eqs. (15) and (16), and again it should be emphasized that the angle between the major principal strain and the fiber direction should be used on the right hand side of Eq. (21).

The optical isoclinic parameters given by Eq. (21) are shown as a function of $\beta$ in Fig. 11. Also shown are measured isoclinic parameters, taken from Ref. 8. The computed and measured isoclinic angles are in fairly good agreement. The

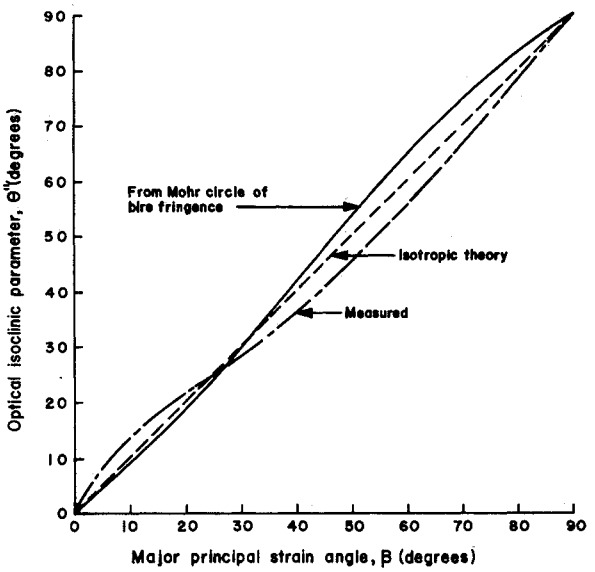


Fig. 11 Optical isoclinic parameters for uniaxial loading.

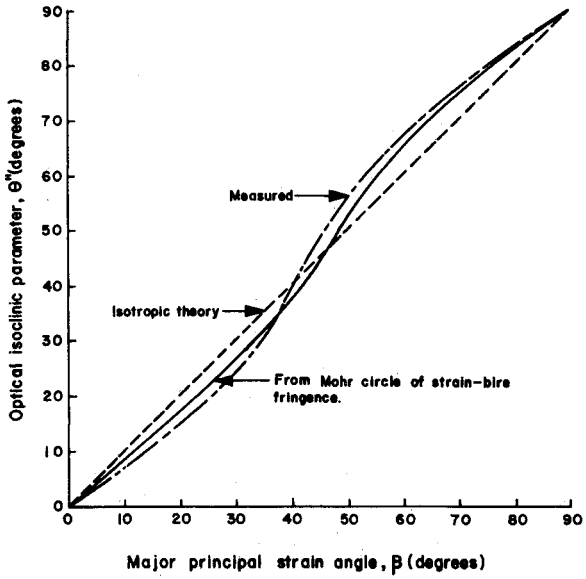


**Fig. 12 Optical isoclinic parameters for biaxial loading.**

angle between the major principal strain and the fiber direction appears to be a good approximation to the measured isoclinic parameter. It has been shown in Ref. 8 that the optical isoclinic parameter is predicted well by the Mohr circle of stress-birefringence, and it is also shown that the major principal strain angle is a very good approximation to the isoclinic parameter.

The optical isoclinic parameters were also computed for the circular disk model from Eq. (20) and the results are shown in Fig. 12. The measured isoclinic parameters, taken from Ref. 8, are also presented and it is seen that the agreement between the two sets of values is good. Again it is observed that the angle between the major principal strain and the fiber direction $\beta$ is a good approximation to the isoclinic parameter.

## Conclusions

The general strain-optic law developed here is rigorous and applicable to all orthotropic birefringent model materials. When an accurate photoelastic analysis is required, either the stress-optic law or the strain-optic law can be employed (as in the case of isotropic model materials). However, when an approximate analysis is sufficient, the strain-optic law, in its simplified form involving an average strain-fringe value, can be used. The isochromatic fringe order can be directly interpreted in terms of the difference in principal strains and such an interpretation is accurate to within about $\pm 20\%$ in most cases. In view of the possible inaccuracies due to fiber misalignment, nonuniform thickness, etc., which may lead to an error of the order of 10% in photo-orthotropic-elastic studies, this does not appear too bad.

The isoclinic fringes can be interpreted directly in terms of the principal strain directions and the error involved in such an interpretation is much less. In effect, the simplified strain-optic law treats the orthotropic model as an isotropic model. It is also interesting to note that while the principal stress-fringe values and the principal elastic constants may be widely different for two model materials, the strain-fringe values do not differ so widely. This is illustrated in Table 1 where the properties of the *E*-glass polyester composite used in this investigation and those of the *S*-glass epoxy composite mentioned in Ref. 9 are compared.

## References

[1] Pih, H. and Knight, C. E., "Photoelastic Analysis of Anisotropic Fiber Reinforced Composites," *Journal of Composite Materials*, Vol. 3, 1969, pp. 94–107.

[2] Sampson, R. C., "A Stress-Optic Law for Photoelastic Analysis of Orthotropic Composites," *Experimental Mechanics*, Vol. 10, May 1970, pp. 210–215.

[3] Dally, J. W. and Prabhakaran, R., "Photo-Orthotropic-Elasticity," Pts. I and II, *Experimental Mechanics*, Vol. 11, Aug. 1971, pp. 346–356.

[4] Prabhakaran, R. and Dally, J. W., "The Application of Photo-Orthotropic-Elasticity," *Journal of Strain Analysis*, Vol. 7, Oct. 1972, pp. 253–260.

[5] Bert, C. W., "Theory of Photoelasticity for Birefringent Filamentary Composites," presented at the Fifth St. Louis Symposium on Advanced Composites, April 1971, St. Louis, Mo.

[6] Prabhakaran, R., "Photoelastic Analysis of an Orthotropic Ring under Diametral Compression," *AIAA Journal*, Vol. 11, June 1973, pp. 777–778.

[7] Prabhakaran, R., "On the Stress-Optic Law for Orthotropic Model Materials in Biaxial Stress-Fields," *Experimental Mechanics*, Vol. 15, Jan. 1975, pp. 29–34.

[8] Prabhakaran, R., "The Interpretation of Isoclinics in Photo-Orthotropic-Elasticity," to be published in *Experimental Mechanics*.

[9] Pipes, R. B. and Rose, J. L., "Photo-Anisotropic-Elasticity: A Strain-Optic Law for Birefringent Composites," presented at the Third International Congress on Experimental Mechanics, May 1973, Los Angeles, Calif.; also *Experimental Mechanics*, Vol. 14, Sep. 1974, pp. 355–360.